An advanced particle filtering algorithm for improving conflict detection in Air Traffic Control

Ioannis Lymperopoulos
Automatic Control Laboratory
ETH Zurich
Zurich, CH-8092, Switzerland
Email: lymperopoulos@control.ee.ethz.ch

Georgios Chaloulos
Automatic Control Laboratory
ETH Zurich
Zurich, CH-8092, Switzerland
Email: chaloulos@control.ee.ethz.ch

John Lygeros
Automatic Control Laboratory
ETH Zurich
Zurich, CH-8092, Switzerland
Email: lygeros@control.ee.ethz.ch

***Abstract*—Enhanced accuracy in aircraft conflict detection allows for more efficient use of the airspace and increased safety levels. Trajectory prediction lies at the heart of most conflict detection algorithms. By comparing the predicted trajectories of different aircraft against each other, we can detect real threats while avoiding false alarms. We show how trajectory prediction tools that account for weather forecast errors can improve the performance of a conflict detection scheme. Using information from multiple aircraft at different locations and time instants, wind forecast uncertainties are reduced increasing trajectory prediction accuracy. We present a particle filtering algorithm that can efficiently cope with the high dimensionality and the non-linearity of the problem and show how using this algorithm can improve considerably conflict detection rates in mid and short term horizon encounters.**

I. Introduction

The current Air Traffic Management (ATM) system is to a large extent based on a rigidly structured airspace and a mostly human-operated system architecture [1]. This could potentially impose a constraint in the growth of air traffic, which is otherwise expected to increase considerably the following years [2]. Recent research efforts focus on integrating the segregated airspace (following SESAR [3] in Europe and NEXTGEN [4] in the US). In support of this effort, a large variety of automation and decision support tools are being developed to provide Air Traffic Controllers (ATCs) with more accurate predictive information about aircraft trajectories, local and national traffic flow, weather and routing.

Guaranteing safety in air travel remains the primary concern in the future ATM. One important aspect in this direction is the separation assurance between flight trajectories. Whenever a prescribed minimum separation between two aircraft is violated, a conflict occurs. For conflicts to be identified and prevented, an automated mechanism for Conflict Detection (CD) is required. Once a conflict is predicted, either a centralized [3] or a decentralized [5] Conflict Resolution (CR) scheme can be used to resolve it; for an overview see [6].

CD is itself a challenging task and very often it is combined with the CR task. Most common methods can be divided into three major categories, based on the prediction horizon they consider. Roughly speaking Long term Conflict Detection and Resolution (CD&R) methods deal with horizons of more than 30 mins. Their main concern is typically flow management problems. Mid term CD&R, accounts for prediction horizons up to 30 mins. Finally, short term CD&R, deals with horizons up to 10 mins.

For the conflict detection to be accurate, one should be able to compute a reliable prediction of the trajectory of an aircraft [7]. Increasing levels of traffic require systems that can accurately predict conflicts earlier, in order to accommodate the extra traffic demand. An automated conflict detection mechanism can take advantage of data that might not be directly accessible, or possibly hard to interpret, by the air traffic controllers, such as the estimated state of the aircraft, weather information and weather uncertainty or different aircraft performance models. This information combined with the data that an air traffic controller has access to, like the estimated position and aircraft flight plans, can lead to an algorithm that improves Trajectory Prediction (TP) and assists the Air Traffic Controller (ATC) in identifying early potential conflicting situations. The longer the horizon the aircraft trajectory is accurately predicted, the more flexibility the ATC (or a conflict resolution algorithm) has to resolve a conflict, or to accommodate more traffic.

Here we demonstrate how CD can be improved by reducing TP inaccuracies related to wind forecast errors. The problem of extracting the wind forecast error information from the trajectories of the aircraft is formulated as a filtering problem. The state that has to be estimated is high dimensional, since it comprises the states (position and heading) of all aircraft in the region of interest, as well as the wind forecast error (projected on a grid). The situation is further complicated by the fact that the aircraft dynamics, through which the wind forecast error is indirectly observed, are nonlinear. This implies that efficient filtering methods (such as the Kalman filter [8]) are inapplicable in this case, whereas methods that could cope with nonlinear dynamics (such as the Particle Filter (PF) [9]) have difficulties dealing with high dimensional states. To solve the problem a novel particle filtering algorithm is developed (called Sequential Conditional Particle Filter (SCPF)) that can deal with both the nonlinear and the high dimensional nature of the problem. For this, the special structure afforded by the filtering problem is exploited, namely the fact that wind forecast error dynamics are linear and conditional on the wind, the dynamics of the different aircraft are independent.

The performance of the proposed algorithm is assessed with a series of simulated feasibility studies. A base scenario involving 2 aircraft flying level with constant airspeed is established. A series of different wind forecast errors is generated which result in potential conflicts. The algorithm shows a significant improvement over the non-filtered wind-forecast especially for the mid-term prediction horizon (20-15 minutes). A further improvement can be achieved when additional aircraft precede the flight of interest.

The rest of the paper is organized as follows. Section II briefly describes the aircraft and wind models used for the simulations. Section III introduces general nonlinear filtering and Particle Filters and outlines the proposed algorithm. Finally, Section IV provides simulation results that document the performance of the proposed method. The paper concludes with Section V which states the conclusions of this study and some ideas for future work.

II. Model Dynamics

We present a Point Mass Model (PMM) that simulates the dynamics of a commercial aircraft from the point of view of an air traffic controller. The model is framed in the context of stochastic hybrid systems and is capable of capturing multiple instances of flights, each with a different flight plan, aircraft dynamics and flight management system. The dynamics capture the effect of the wind and the wind forecast error, which is treated as a stochastic disturbance to the model.

A. Aircraft Dynamics

The model presented here concentrates on level flights with constant airspeed and is a simplified version of a full model (including varying airspeed, altitude, and control of flight path angle) developed in our earlier work [10], [11]. The dynamics of the aircraft are characterized by the following state vector $z = [\ X,\ \ Y,\ \ \psi,\ \ m,\ ] \in \mathbb{R}^4$ where X and Y are the position of the aircraft in the West-East and South-North direction, respectively, m denotes the mass of the aircraft and ψ its heading. We assume that each aircraft flies with known, constant True Airspeed (TAS) which depends on aircraft type and altitude. Figure 1 depicts the major variables of the model. The relation between the states is nonlinear and depends also on the actions of the Flight Management System (FMS). The values of different parameters (for example the TAS, the lift and drag coefficients, or fuel burn coefficient) which depend on aircraft type, the phase of flight and aircraft configuration are obtained from the Base of Aircraft Data (BADA) database [12]. The movement of the aircraft is also affected by the wind which acts as a disturbance. Thus, the equations of motion, for level flight, become

$$\begin{bmatrix} \dot{X}(t) \\ \dot{Y}(t) \\ \dot{\psi}(t) \\ \dot{m}(t) \end{bmatrix} = \begin{bmatrix} V\cos(\psi(t)) + w_X(t) \\ V\sin(\psi(t)) + w_Y(t) \\ \dfrac{C_L S \rho(Z) V \sin(\phi(t))}{2m(t)} \\ -\eta T(t) \end{bmatrix}. \quad (1)$$

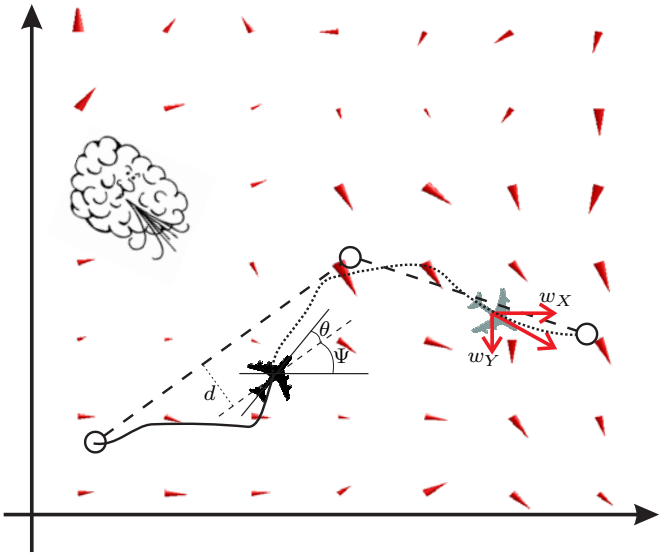

Fig. 1. The aircraft FMS tracks the flight plan between two subsequent way-points, in the presence of wind. The cones represent the direction and magnitude of the wind at different locations. Ψ denotes the nominal heading.

C_L is the lift coefficient, S represents the surface of the wings, $\rho(\cdot)$ the air density depending on altitude (Z). While V is the true airspeed, (ϕ) the bank angle and η the fuel burn coefficient. The values of the parameters (including the TAS) which depend on aircraft type, the phase of flight and aircraft configuration are obtained from the BADA database [12].

B. Flight Management System

The FMS measures the state of the aircraft and guides it along the flight plan by determining the values of the inputs. One of its two components is controlling along track and vertical motion (in our case maintaining constant altitude and airspeed) through the thrust and flight path angle and the other is controlling cross track motion through the bank angle. To ensure constant airspeed the thrust is set equal to the drag force, whereas to ensure level flight we assume that the flight path angle is set to zero. The bank angle is set using a nonlinear feedback controller which corrects cross track deviations from the flight plan encoded through heading (θ) and cross-track errors (d) in Figure 1. Details of the design of these controllers are given in [10], [11]. The aircraft dynamics and the control inputs applied by the FMSare affected by a change in the discrete part of the dynamics. The discrete dynamics arise from the flight plan of the aircraft and the logic variables embedded in the FMS. For more details the reader is referred to [10]–[12].

C. Radar Model

The position of all aircraft is measured using a ground radar. We assume that the radar measurements are corrupted by noise. In practice the accuracy of the radar usually decreases as an aircraft moves away from the radar location. For simplicity, we use the same measurement error statistics for all distances,

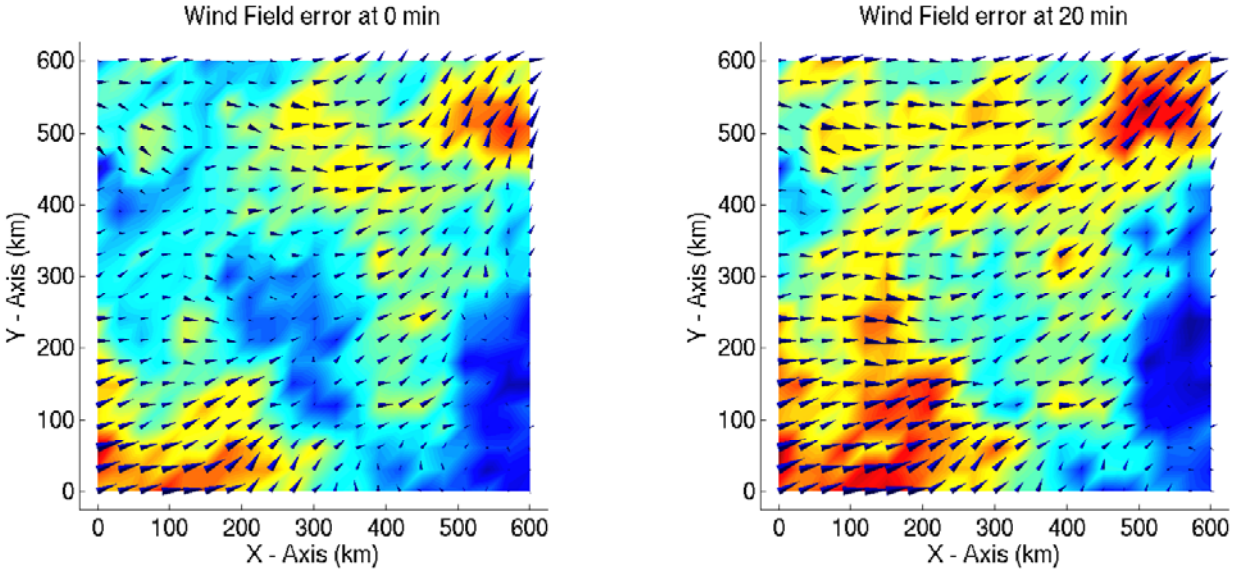

Fig. 2. Example of wind forecast error on a single flight level. The intensity of the color from blue to red indicates a low to high wind forecast error magnitude respectively. The left image displays the initial wind-field. while the right the evolution of the wind-field after 20 minutes. The horizontal grid resolution is 30x30km

and select the variance high enough ($\sigma_r = 80$m) to ensure we err on the side of caution.

D. Wind Model

The uncertainty in the flight trajectory is greatly affected by inaccurate meteorological forecasts [13], [14]. We model the wind as a sum of two components: a nominal component (representing weather forecasts) and a stochastic component (representing forecast errors).

1) Wind Forecast: The nominal part of the wind-field represents the meteorological predictions that are available to the ATC. We obtain those meteorological data from the Rapid Update Cycle (RUC), a numerical weather prediction model for the U.S.A. [15]. The RUC model is run every three hours and each run produces a set of three hourly forecasts.

2) Wind Forecast Error Statistics: We model the wind forecast errors as a random field: $w : \mathbb{R} \times \mathbb{R}^3 \rightarrow \mathbb{R}^2$ where $w(t, P)$ represents the wind at point $P \in \mathbb{R}^3$ and at time $t \in \mathbb{R}$. Since we restrict attention to level flights we ignore wind in the vertical direction. For simplicity, here we restrict attention to the case where $w(t, P) \in \mathbb{R}^2$ is Gaussian with zero mean and covariance matrix $R(t, P, t', P') \in \mathbb{R}^{2\times 2}$. We calculate the covariance matrix, describing the spatiotemporal correlation of the forecast error based on [16]. The correlation decays exponentially with horizontal distance, altitude and time difference. The data suggest a strong correlation between wind errors in the same horizontal plane, a very strong correlation in time and a weaker correlation across different altitudes.

To describe the wind-field we grid the airspace into a lattice comprising N_X points in the South-North direction, N_Y points in the East-West direction and N_Z points vertically. For each grid point in the lattice we generate two random numbers, one for the South-North and one for the East-West direction of the wind forecast error. We store these numbers in two vectors $W_X(k)$ and $W_Y(k)$, at time step $k \in \mathbb{N}$ (every δ_t seconds). An example of the horizontal part of the lattice can be seen in Figure 2.

Let $\hat{R} \in \mathbb{R}^{N_X N_Y N_Z \times N_X N_Y N_Z}$ denote the covariance matrix of $W_X(k)$ (by the isotropic assumption, the matrix will be identical for $W_Y(k)$). We generate wind samples using the following linear Gaussian model

$$\begin{aligned} W_X(0) &= \hat{Q} v_X(0), \quad W_X(k+1) = aW_X(k) + Q v_X(k+1), \\ W_Y(0) &= \hat{Q} v_Y(0), \quad W_Y(k+1) = aW_Y(k) + Q v_Y(k+1), \end{aligned} \tag{2}$$

where $v_X(k), v_Y(k) \in \mathbb{R}^{N_X N_Y N_Z}$ are standard (zero mean, identity covariance matrix) independent Gaussian random variables. Q and $\hat{Q}$ are derived by Cholesky Decomposition from the covariance matrix $\hat{R}$ according to

$$QQ^T = (1 - a^2)\hat{R} \text{ and } \hat{Q}\hat{Q}^T = \hat{R}. \tag{3}$$

It is easy to show that the covariance matrices of the resulting vectors for an appropriate choice of a (we set $a = e^{-\delta_t/G_t} \in \mathbb{R}$, where G_t is a parameter of the time correlation [16]) closely resemble the structure implied by the spatiotemporal correlation. Linear interpolation of the wind at the neighboring grid points is used to compute the wind forecast error between the grid points, details can be found in [17].

III. Nonlinear Filtering

Problems in engineering applications often require the accurate estimation of the state of a system that evolves in time, using a sequence of noisy observations that become available

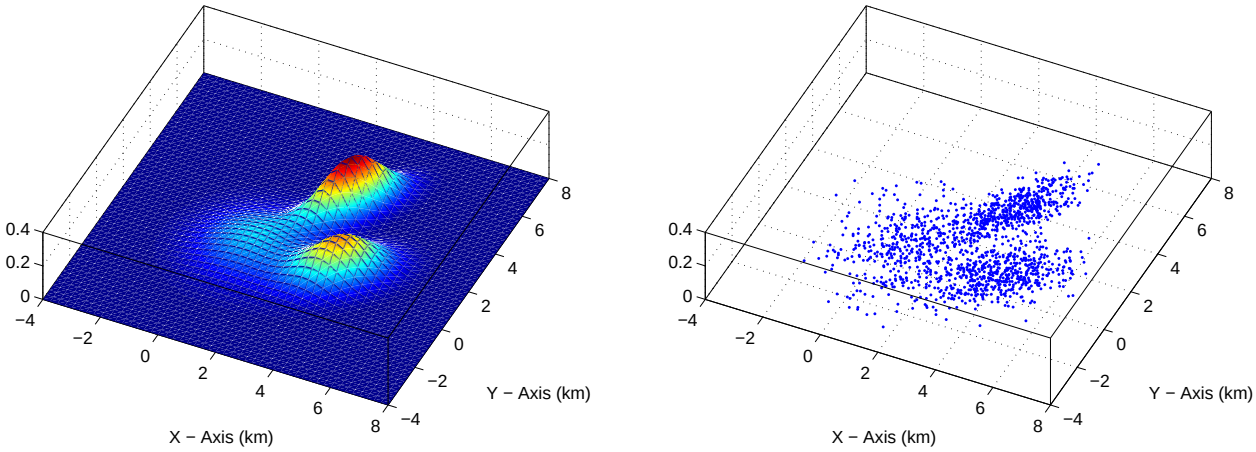

Fig. 3. Example of continuous probability density function (left) and its particle approximation (right). The location and weight of the particles reflect the value of the probability density in that region of the state space.

on-line. For several cases, it is important to include elements of nonlinearity and non-Gaussianity in order to accurately capture the underlying dynamics of the physical system. Moreover, for real time performance it is usually required to process data as they arrive, both from the point of view of storage but mainly for keeping the computational complexity manageable. Filtering algorithms perform such on-line data assimilation to generate estimates of the state [18], [19].

The starting point is typically a discrete time model of the dynamics of the process and the measurements of the form

$$\begin{array}{rcl} x(k+1) & = & f(x(k), v(k), k) \\ y(k) & = & h(x(k), n(k), k), \end{array} \tag{4}$$

where $x(k) \in \mathbb{R}^n$ and $y(k) \in \mathbb{R}^p$ are the state and output of the system at time $k \in \mathbb{N}$, and $f : \mathbb{R}^n \times \mathbb{R}^n \times \mathbb{N} \to \mathbb{R}^n$ and $h : \mathbb{R}^n \times \mathbb{R}^p \times \mathbb{N} \to \mathbb{R}^p$ are (possibly nonlinear) functions. $v(k) \in \mathbb{R}^n$ and $n(k) \in \mathbb{R}^p$ are process and measurement noise, which are generally assumed to be independent, identically distributed stochastic processes, but not necessarily additive, or Gaussian. We also assume that the initial state is independent of the noise processes and its distribution is given through a Probability Density Function (pdf) $p(x(0))$. If the pdf of the noise processes are known, the system of can be equivalently represented using two pdf

$$\begin{array}{rcl} x(k) & \sim & p_x(\cdot|x(k-1), k) \\ y(k) & \sim & p_y(\cdot|x(k), k) \ . \end{array} \tag{5}$$

Here $p_x(\cdot|x(k-1), k)$ is a conditional pdf that models the stochastic dynamics of the state of the system, determined by f and the pdf of $v(k)$, while $p_y(\cdot|x(k), k)$ is a conditional pdf that models the probability distribution of the measurements, determined by h and the pdf of $n(k)$.

Given $k, k' \in \mathbb{N}$ let $\mathbb{Y}(k') = \{y(i)\}_{i=0,\ldots,k'}$ denote the sequence of measurements up to time k' and $\mathbb{X}(k) = \{x(i)\}_{i=0,\ldots,k}$ denote the sequence of states up to time k. The aim is to estimate the pdf $p(\mathbb{X}(k)|\mathbb{Y}(k'))$. This density function embodies our best estimate of the state vector up to time k given all available information up to time k'. Depending on the relation of k to k' we can formulate three different types of estimation problems; **Filtering** ($k = k'$), **Prediction** ($k > k'$), **Smoothing** ($k < k'$). These can be solved recursively by invoking Bayes' theorem.

A. Particle Filters

The analytical solution of the optimal Bayesian estimate is not always possible, since the integrals involved are seldomly tractable. In the general case we need to approximate numerically the pdf of interest. Particle filters (or Sequential Monte Carlo methods [9]) are fast estimation techniques that perform this numerical approximation using simulation. The main idea is to approximate the continuous probability distribution of interest using a discrete distribution comprising weighted samples (known as particles, Figure 3). To do this we extract N independent identically distributed particles, $\mathbb{X}^1(k), \ldots, \mathbb{X}^N(k)$ from $p(\mathbb{X}(k)|\mathbb{Y}(k))$, and construct an empirical estimate of the distribution

$$\hat{p}(\mathbb{X}(k)|\mathbb{Y}(k)) = \frac{1}{N}\sum_{i=1}^{N} \delta_{\mathbb{X}^i(k)}(\mathbb{X}(k)) \ , \tag{6}$$

where $\delta_{\mathbb{X}^i(k)}$ denotes the Dirac mass at particle $\mathbb{X}^i(k)$. We can then approximate the expectation of any integrable function, g, by

$$E[g(\mathbb{X}(k), k)] \approx \int g(\mathbb{X}(k), k)\hat{p}(d\mathbb{X}(k)|\mathbb{Y}(k)) \tag{7}$$

$$= \frac{1}{N}\sum_{i=1}^{N} g(\mathbb{X}^i(k), k) \ . \tag{8}$$

It can be shown that this estimator is unbiased and (under weak assumptions) converges to the true expectation as the number of particles N tends to infinity [20].

Particle filters suffer from what is known as curse of dimensionality [21] which makes their use in high dimensional

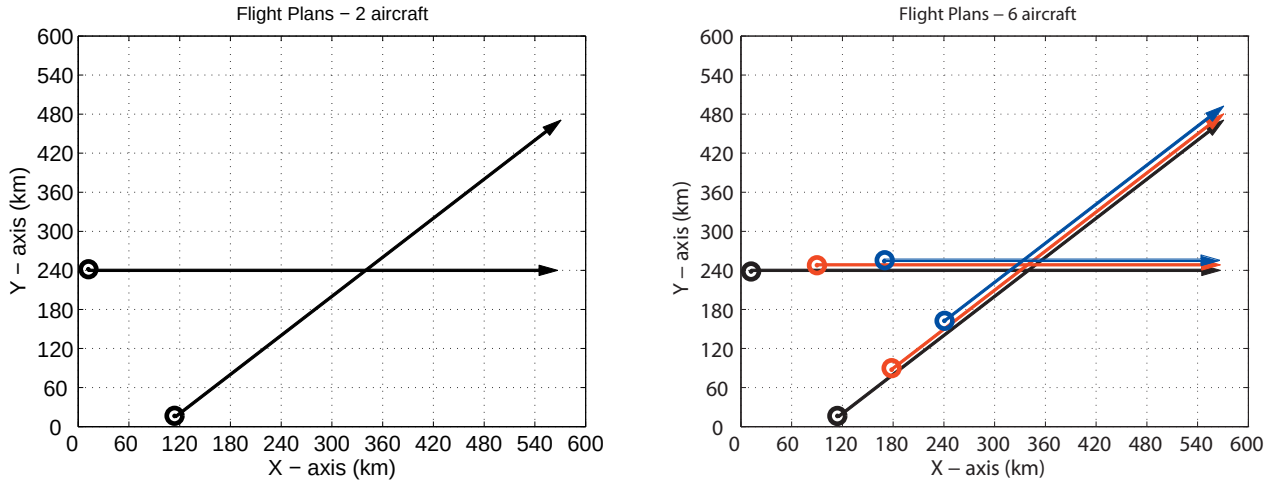

Fig. 4. Flight plans for two (left) and 6 aircraft (right).

problems difficult. Our simulations suggest that most particle filtering algorithms cannot handle efficiently both the high dimensionality of the wind state and the nonlinearities in multi-aircraft dynamics [22].

B. Sequential Conditional Particle Filter

To solve the problems linked to particle filtering we have developed a novel algorithm (which we call Sequential Conditional Particle Filter (SCPF), first introduced in [17]) that can deal with both the nonlinear and the high dimensional nature of the problem. To achieve this we exploit the special structure of the problem, namely the fact that wind forecast error dynamics are linear and that, conditional on the wind, the dynamics of the different aircraft are independent. The SCPF shares some of the insights of the Marginalized Particle Filter (MPF) [23], in the sense, that both treat the linear and the non-linear part of the state separately. The two main novelties compared with the MPF is the sequential incorporation of information from different aircraft and the substitution of particles carrying uncertainty realizations by particles carrying conditional distributions.

The algorithm exploits the fact that the aircraft states evolve according to non-linear dynamics, while the wind states evolve according to linear dynamics. Moreover, the evolution of the wind states is independent of the evolution of the aircraft states and the evolution of the states of different aircraft are only coupled to each other only through the wind states. The first two observations imply that the wind states should be easier to estimate, since under Gaussianity assumptions, storing and manipulating them only requires keeping track of their mean and covariance matrix. Moreover, given a probabilistic estimation of the wind at some points in the wind-field, we can explicitly derive the conditional distribution of the wind at all other points. This distribution will also be Gaussian, hence easy to store and manipulate. This way every aircraft acts as an indirect local sensor of the wind. The first novelty of the proposed algorithm is that, instead of using realizations for the wind states in our particles (as in conventional particle filtering) we store and manipulate the entire conditional probability distribution. The latter two observations imply that, conditional on the wind states, the states of different aircraft are independent of each other. This is exploited by the second novelty of our algorithm, which is the sequential incorporation of the information from different aircraft. Every radar measurement contains information about the positions, of all aircraft in a region of the airspace, but new measurements are processed one aircraft at the time. The complete algorithm is reported in [17].

IV. Simulation Results

We have devised a series of simulations to demonstrate the performance of the new algorithm. Two aircraft approach each other with an angle of 45^o. Nominally, without any wind forecast error, the two aircraft exhibit minimum separation (5nmi) after 25 minutes of flight. To demonstrate the algorithm can also exploit information from additional aircraft that happen to be present in the airspace we have created an additional scenario with 6 aircraft in total. The flight plans for the two cases can be seen in Figure 4.

Aircraft fly level at $10000m$ altitude with a nominal airspeed of 419 knots, and there are no turns included in the flight plans. The parameters of the dynamical models for all aircraft represent a Boeing 737-700. Flights have a duration of approximately 30 minutes and radar measurements arrive every 30 seconds. We simulate these flights under 1000 different wind forecast error realizations. Figure 5 demonstrates the significance of the forecast error. The different scenarios exhibit, on average, their minimum separation after 25 minutes ($1500s$) as in the nominal case, but the range is now from 1440 to $1570s$. For the same flight plan, there exist wind forecast errors for which the separation drops to 0.03 nmi and others for which it reaches 14 nmi. In total, out of the 1000 scenarios, 509 will result in conflict (conflict is $5nmi$).

In order to benchmark the efficiency of the algorithm we

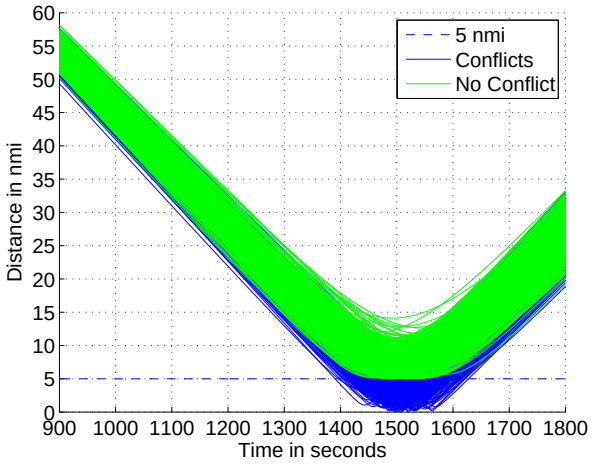

Fig. 5. Time evolution of the separation between the two aircraft for different scenarios of wind forecast errors. Blue lines represent conflicts and green lines represent scenarios where a safe separation distance was kept throughout the flight.

compare with two benchmarks. The first one (called "agnostic") evaluates the conflict detection rates with only wind forecasts available, without any filtering performed. This is the general case in current practice. The second (called 'perfect') evaluates the conflict rates given perfect information about the wind-field all over the airspace at the current point in time. The TP uncertainty in this case is only due to the time evolution of the wind-error, which is unpredictable given the current state. This is clearly an unrealistic, perfect filtering situation and constitutes an optimal, best case performance bound for the proposed algorithm.

The algorithm is run using 1000 particles for the 2 and 6 aircraft case for each of the 1000 wind forecast error scenarios. Having used the algorithm to filter $5, 10$ and 15 minutes of data (so 20,15 and 10 minutes before estimated time of minimum separation) we extrapolate the state estimate of all particles into the future to get an estimate of the future trajectory for each aircraft. We calculate, for each particle the distance of the two aircraft for every second and evaluate the minimum separation throughout the flight. Since each particle will exhibit a different minimum separation, there will be particles for which a conflict has occurred and particles with no conflict for the same wind forecast error scenario. We use the ratio of particles with conflict over the total number of particles as our estimate for the probability of conflict for this scenario.

The results are presented as distributions, using histograms. For each scenario, the algorithm estimates a probability of conflict. We display the results for the scenarios where a conflict actually happened in Figure 6. A distribution skewed to the right implies that most of the conflicts (out of the 509) where identified with high probability. The perfect case would be all 509 cases in the $95 - 100\%$ probability bin. For the scenarios that are placed in each bin the average minimum separation is computed. Minimum separation is defined as the minimum distance throughout the flight, for the real scenarios.

The agnostic case predictions, Figure 6(a), for 20 and 15 minutes before estimated conflict provide a quite flat distribution. This implies that most of the conflicts are not identified with high probability. The improvement over the agnostic case even only after 5 minutes of flight (20 minutes before conflict) is quite strong for 2 aircraft and becomes even greater when we employ 6 aircraft. This continues for 10 and 15 minutes of filtering and shows the contribution of more aircraft in the airspace. However, after 15 minutes of filtering, adding more aircraft does not significantly increase the conflict detection rate. It is important to note that the 6 aircraft case is not far from the upper margin of performance indicated by the perfect information case, Figure 6(d). Note that even 10 minutes before the conflict there still exist conflicts that are not well identified. SCPF for some cases provides an estimate of the probability of conflict as low as 10-20%. This is due to the conflict being marginal, between 4.5 and $5nmi$, Figure 6. Accepting conflicts that breach 5.5 or $6nmi$, would increase margins, with an increase of false alarms of course, but in some cases, this might be a suitable trade-off.

Finally, Figures 7, 8 (including all wind realizations) show how the algorithm improves the estimation of the minimum separation and the time at which it occurs. Standard deviation for minimum separation error is 1.03 nmi and $11s$ for time error in the agnostic case, while this improves to 0.36 nmi and $2.7s$ for the 6 aircraft SCPF case. The ideal bound is 0.18 nmi and $1.9s$ for the perfect information case.

By choosing a probability threshold after which a scenario is considered a conflict we can also estimate the false alarm and successful alert probabilities. The following table shows the result 10min before conflict for a threshold of 90%.

90% Threshold (Agnostic - **6-SCPF** - Perfect)		
	Conflict	No Conflict
Alert	51% - **80**$\%$ - 94%	51% - **22**$\%$ - 7%
No Alert	49% - **20**$\%$ - 6%	49% - **78**$\%$ - 93%

We observe quite a significant increase in the successful alarms and respectively a decrease in false alarms when the SCPF with 6 aircraft is employed, over the agnostic case.

V. Conclusion

A method for improving conflict detection (CD) was presented. The performance of the algorithm was tested in flight plans including 2 and 6 aircraft. CD was improved considerably using SCPF compared with the agnostic case where no inference about the forecast error was made. The proposed method manages to both increase the successful alerts and reduce false alerts. Finally, simulations show how the error in the estimates of minimum separation and time to minimum separation are reduced.

Acknowledgment

The authors gratefully acknowledge the contribution of the European Commission through project iFLY, FP6-TREN-037180. The authors would like to thank K. Koutroumpas for helpful discussions and comments.

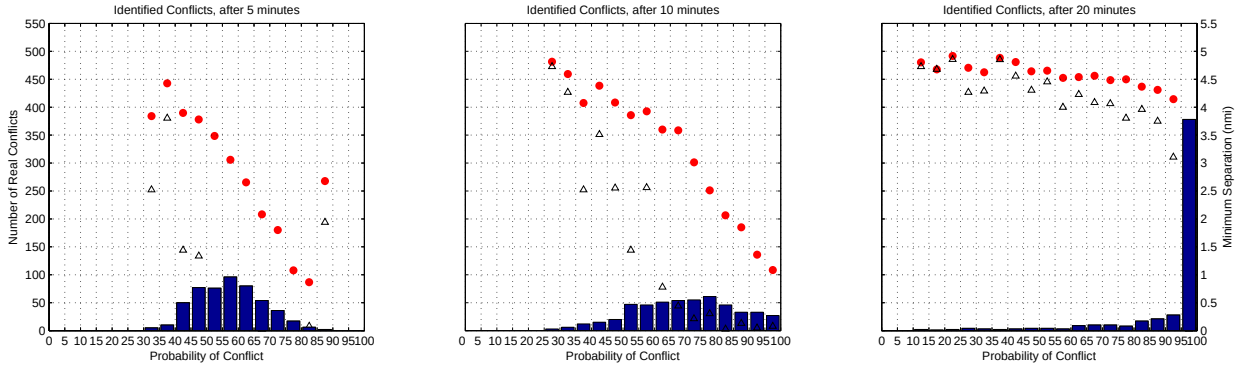

(a) Only meteorological forecasts available

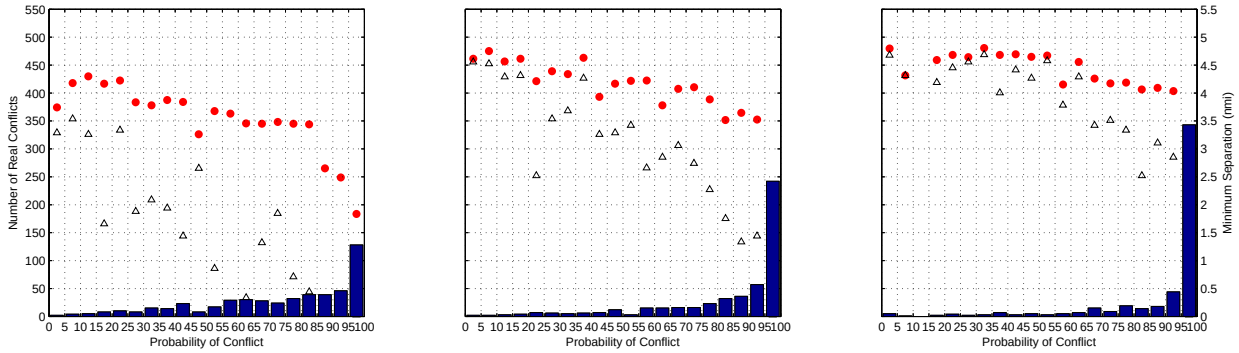

(b) SCPF with 2 aircraft

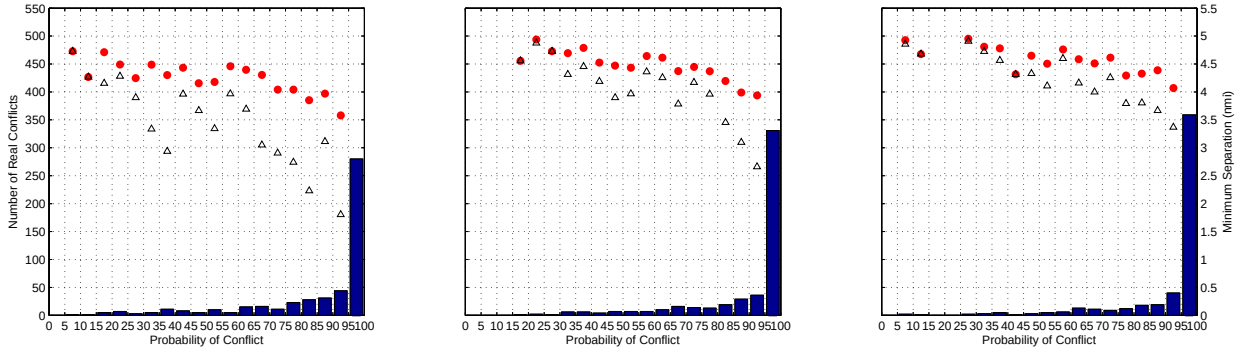

(c) SCPF with 6 aircraft

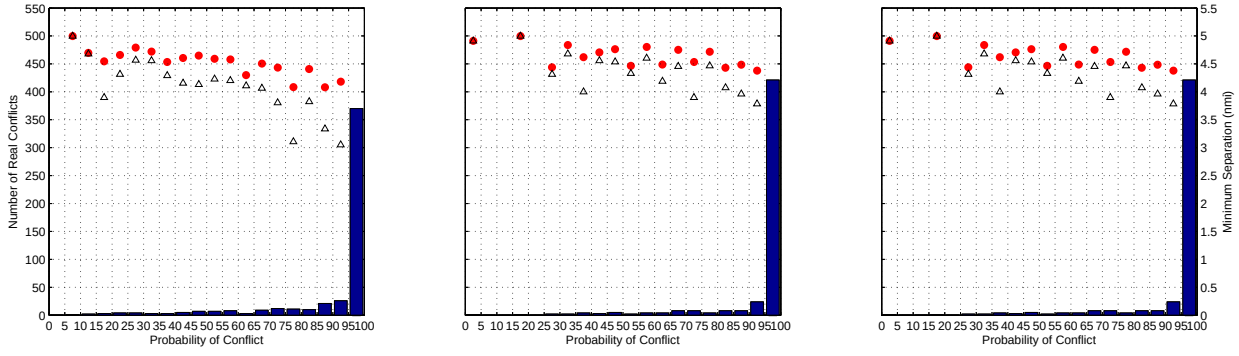

(d) Perfect information available

Fig. 6. Evolution of the conflict probability after 5 (left), 10 (middle), 15 (right) minutes of filtering, for scenarios where a conflict occurred. Red dots show the average minimum separation distance for each percentage bin and black triangles the minimum among them - 500 signifies 5nmi for this metric.

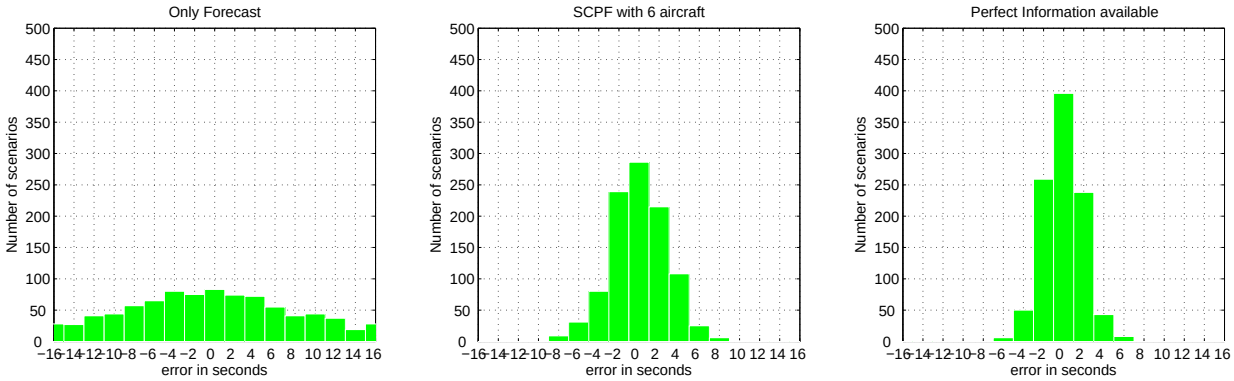

Fig. 7. Distribution of the time error to minimum separation after 15 minutes of filtering for different algorithms

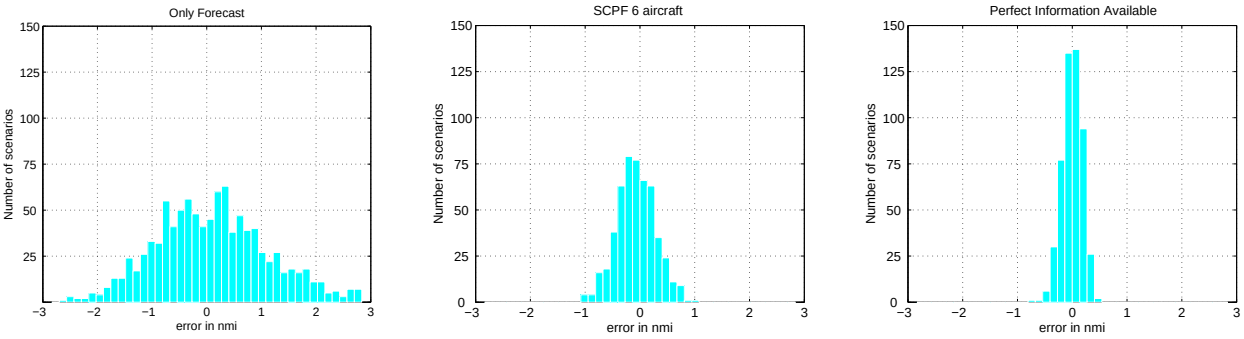

Fig. 8. Distribution of the distance error for minimum separation after 15 minutes of filtering for different algorithms

REFERENCES

[1] M. Nolan, *Fundamentals of Air Traffic Control*, 3rd ed. Belmont, CA: Wadsworth: Wadsworth Publishing Company, 1998.

[2] Department of Transport, "UK Air passenger demand and CO2 forecasts 2009," UK, Tech. Rep., January 2009, http://www.dft.gov.uk/pgr/aviation/atf/co2forecasts09/.

[3] SESAR Joint Undertaking, "SESAR (Single European Sky ATM Research)," 2007, http://www.sesarju.eu/.

[4] NEXTGEN, "Concept of Operations for the Next Generation Air Transport System," 2007, http://www.jpdo.gov/library/NextGen_ v2.0.pdf.

[5] G. Cuevas, I. Echegoyen, J. García, P. Cásek, C. Keinrath, F. Bussink, and A. Luuk, "Autonomous Aircraft Advanced (A3) ConOps," iFly Project, Tech. Rep. Deliverable D1.3, 2008.

[6] J. Kuchar and L. Yang, "A review of conflict detection and resolution methods," *IEEE Transactions on Intelligent Transportation Systems*, vol. 1, no. 4, pp. 179–189, 2000.

[7] I. Lymperopoulos and J. Lygeros, "Adaptive Aircraft Trajectory Prediction using Particle Filters," in *AIAA Guidance, Navigation and Control Conference and Exhibit*, Honolulu, Hawaii, August 2008.

[8] T. Kailath, A. H. Sayed, and B. Hassibi, *Linear estimation*, ser. Information and System Sciences. Prentice Hall, NJ, 2000.

[9] A. Doucet, J. F. G. D. Freitas, and N. J. Gordon, *Sequential Monte Carlo Methods in Practice*, ser. Statistics for Engineering and Information Science. New York: Springer Verlag, 2001.

[10] W. Glover and J. Lygeros, "A stochastic hybrid model for air traffic control simulation," in *Hybrid Systems: Computation and Control*, ser. LNCS, R. Alur and G. Pappas, Eds. Springer Verlag, 2004, no. 2993, pp. 372–386.

[11] I. Lymperopoulos, A. Lecchini, W. Glover, J. M. Maciejowski, and J. Lygeros, "A stochastic hybrid model for air traffic management processes," University of Cambridge, Tech. Rep. CUED/F-INFENG/TR.572, February 2007.

[12] Eurocontrol Experimental Centre, "User Manual for the Base of Aircraft Data (BADA) revision 3.3," 2002, http://www.eurocontrol.fr/projects/bada/.

[13] S. G. Benjamin, B. E. Schwartz, and R. E. Cole, "Accuracy of ACARS wind and temperature observations determined by collocation," *Weather and Forecasting*, vol. 14, pp. 1032–1038, 1999.

[14] M. R. C. Jackson, Y. J. Zhao, and R. A. Slattery, "Sensitivity of Trajectory Prediction in Air Traffic Management," *AIAA Journal of Guidance, Control, and Dynamics*, vol. 22, no. 2, pp. 219–228, 1999.

[15] Earth System Research Laboratory, "Rapid update cycle (RUC)," 2007, http://ruc.noaa.gov/.

[16] R. E. Cole, C. Richard, S. Kim, and D. Bailey, "An assessment of the 60 km rapid update cycle (RUC) with near real-time aircraft reports," MIT Lincoln Laboratory, Tech. Rep. NASA/A-1, July 15, 1998.

[17] I. Lymperopoulos and J. Lygeros, "Improved Multi-Aircraft Ground Trajectory Prediction for Air Traffic Control," *AIAA, Journal of Guidance Control and Dynamics*, vol. 33, no. 2, pp. 347–362, 2010.

[18] A. H. Jazwinski, *Stochastic processes and filtering theory*, ser. Mathematics in Science and Engineering. New York: Academic Press, 1970, vol. 64.

[19] M. S. Arulampalam, S. Maskell, N. J. Gordon, and T. Clapp, "A tutorial on particle filters for online nonlinear/non-gaussian bayesian tracking," *IEEE Transactions on Signal Processing*, vol. 50, no. 2, pp. 174–188, 2002.

[20] D. Crisan and A. Doucet, "A survey of convergence results on particle filtering methods for practitioners," *IEEE Transactions on Signal Processing*, vol. 50, no. 3, pp. 736–746, 2002.

[21] F. Daum and J. Huang, "Curse of dimensionality and particle filters," in *Aerospace Conference, 2003. Proceedings. 2003 IEEE*, vol. 4, Montreal,Quebec, Canada, September 2003, pp. 1979– 1993.

[22] I. Lymperopoulos and J. Lygeros, "Sequential monte carlo methods for multi-aircraft trajectory prediction in air traffic management," *International Journal of Adaptive Control and Signal Processing*, 2010, to appear.

[23] T. B. Schön, F. Gustafsson, and P. J. Nordlund, "Marginalized particle filters for mixed linear/nonlinear state-space models," *IEEE Transactions on Signal Processing*, vol. 53, no. 7, pp. 2279– 2289, 2005.